Ceramics International 46 (2020) 11747–11761

Contents lists available at ScienceDirect

Ceramics International

journal homepage: www.elsevier.com/locate/ceramint

Fabrication of grooves on polymer-derived SiAlCN ceramics using femtosecond laser pulses

Yigao Chen[a], Yejie Cao[a,*], Yiguang Wang[b,**], Ligong Zhang[c], Gang Shao[d], Jinfeng Zi[e]

[a] Science and Technology on Thermostructure Composite Materials Laboratory, Northwestern Polytechnical University, Xi'an, 710072, Shaanxi, China
[b] Institute of Advanced Structure Technology, Beijing Institute of Technology, Haidian District Beijing, 100081, China
[c] State Key Laboratory of Luminescence and Applications, Changchun Institute of Optics, Fine Mechanics and Physics, Chinese Academy of Sciences, Changchun, 130033, Jilin, China
[d] School of Materials Science and Engineering, Zhengzhou University, Zhengzhou, 450001, China
[e] Xi'an MicroMach Technology co., Ltd, Xi'an, 710072, Shaanxi, China

ARTICLE INFO

Keywords:
Polymer-derived ceramics
Femtosecond laser pulse
Groove
Laser-induced periodic surface structures

ABSTRACT

In this study, grooves were fabricated on the surface of fully dense polymer-derived SiAlCN ceramics. Industrial femtosecond laser source was used at wavelength of 1030 nm with pulse duration of 290 fs and repetition rate of 100 kHz. Moreover, comprehensive study was carried out to evaluate the influence of scan speed and energy fluence on grooves quality, including the heat-affected zone around the laser-machined grooves, microstructures of laser-irradiated surface, and cross-section morphology of grooves. A series of grooves with width in the range of 30–80 μm and depth below 280 μm was successfully fabricated using femtosecond laser pulse. Laser parameters were optimized to obtain grooves with satisfying surface quality. Furthermore, formation and disappearance of laser-induced periodic surface structures were systematically investigated. This study proposes fabrication of grooves on SiAlCN ceramics via laser processing, which provides precise method for fabrication of microstructure with fascinating properties.

1. Introduction

Polymer-derived ceramics (PDCs) are semiconductor silicon (Si)-based materials, with potential applications in the field of sensors because of their excellent properties, such as high-temperature stability and oxidation/corrosion resistance [1,2]. Noteworthy, polymer-derived silicon carbonitride (SiCN) ceramics have been developed as one of the best candidates for a high-temperature micro-electric mechanical system (MEMS) via lithography techniques and micro-casting [3,4]. Nonetheless, these methods are inherently challenging as they demand complex equipment and tedious processing steps, and as-fabricated PDC microstructures are easily deformed and develop cracks after pyrolysis. Moreover, the engineering applications of PDC MEMS involving the fabrication and use of some microstructures (including grooves [5–7] and periodic ripples [8]) to form microchannels [9,10] or microfluidic [11] devices have been increasing rapidly. However, the PDCs become hard and brittle after pyrolysis, thus processing these microstructures on PDCs by conventional methods is also limited. Therefore, a novel method for fabricating grooves on PDCs must be thoroughly studied for practical applications.

Recently, ultrashort laser pulse machining has been employed as a precision micromachining technique that is useful for fabricating microstructures and for ablating and machining a wide variety of materials including polymers, metals, and ceramics [12–14]. Notably, use of a femtosecond laser is highly efficient and results in less thermal and mechanical deformation compared to the efficiency and results of using a picosecond and nanosecond laser [15,16]. According to literature, femtosecond laser machined grooves were successfully fabricated on poly (methyl methacrylate) substrates and glass, and the laser incident power and scanning speed exhibited an important role in deciding the main features (depth and width) of the grooves produced by using the laser [17]. Furthermore, the laser-machined grooves on Si were systematically investigated as a function of the variation of pulse energy, translation speed, and number of samples passes [18]. The results revealed three ablation regimes with different ablation rates, and distinct grooves morphology with significant branching in deep grooves. Therefore, femtosecond laser processing has been considered as a promising technique for fabricating grooves with different structural morphologies on the surface of PDCs.

In this study, a femtosecond laser pulse was introduced for

* Corresponding author. Xi'an, Shaanxi, China.
** Corresponding author. Beijing, China.
E-mail addresses: caoyejie@hotmail.com (Y. Cao), wangyiguang@bit.edu.cn (Y. Wang).

https://doi.org/10.1016/j.ceramint.2020.01.209
Received 27 November 2019; Received in revised form 20 January 2020; Accepted 22 January 2020
Available online 25 January 2020

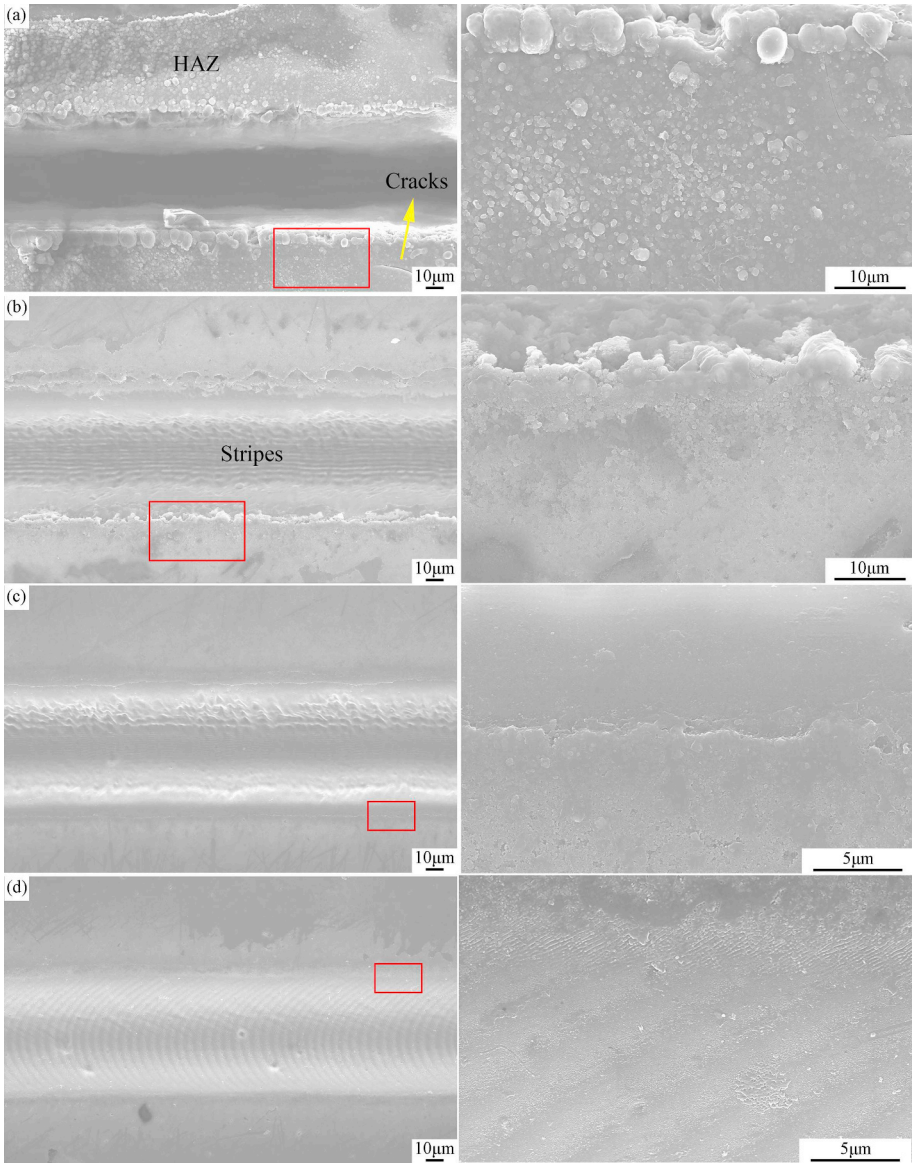

Fig. 1. SEM micrographs of the surface of laser-machined grooves at 11.43 J cm^{-2} with different scan speeds: (a) 50, (b) 150, (c) 250, and (d) 500 mm s^{-1}. Photos in right column are the enlarge photos of the labelled areas in left column.

fabricating grooves on the surface of PDCs, and aluminum (Al)-doped SiCN (SiAlCNs) ceramics were selected as the target PDC materials because of their low porosity and high oxidation/corrosion resistance [19]. A series of grooves was fabricated with different scanning speeds and energy fluence. Scanning electron microscopy (SEM) was used to characterize the surface and cross-section morphology of the samples. The influences of laser parameters on the heat-affected zone (HAZ) around the grooves and generation and disappearance of laser-induced periodic surface structures (LIPSSs) on the irradiated surface were studied in detail. Furthermore, the interaction between femtosecond laser and structuring of amorphous SiAlCN ceramics was comprehensively presented, which lay a foundation for the laser machining of PDCs. As a result, this study is beneficial for the fabrication of different PDC-based devices and their surface modification.

2. Experimental

2.1. Preparation of SiAlCN

SiAlCN precursor was successfully fabricated using commercially available polysilazane (Ceraset, Kion, Huntingdon Valley, PA, USA) and aluminum isopropoxide ($Al[OCH(CH_3)_2]_3$, AI, ACROS ORGANICS, ThermoFisher, USA) (90:10 wt ratio). The resulting mixture was continuously stirred at 120 °C for 6 h. Dicumyl peroxide (DCP, 2 wt%) was then added to accelerate the cross-linking and allow for sufficient dispersion under stirring at room temperature. Noteworthy, the bubbles were thoroughly removed under vacuum for 12 h. Further, translucent polymer rods were obtained on Teflon molds at 130 °C for 4 h. A disc with thickness of 1–1.5 mm was cut using a low-speed diamond saw (SYJ-150, MTI Corporation, CA, USA), and then the discs were pyrolyzed at 1000 °C for 4 h in a tube furnace (GXL-1100X, MTI Corporation) under nitrogen protection. Completely dense SiAlCN ceramic wafers with a thickness of 0.5–1 mm and diameter of 9 mm were obtained, which were polished to a roughness of less than 10 nm and cleaned in an ultrasonic bath.

2.2. Laser machining experiments

Four-axis ultrafast laser micromachining platform (LMM-50, Xi'an MicroMach Technology Co., Ltd., China) was used for laser processing

herein. A femtosecond laser pulse was generated using a regenerative amplified ytterbium-doped solid-state ultra-fast laser system. The wavelength was 1030 nm, the pulse duration was 290 fs, and the repetition rate was 100 kHz. The spot size with diameter of about 35 μm was focused on the surface of the samples using an aspheric lens with a focal length of 116.7 mm. The average power of the laser spot was in the range of 0.1–10 W and it exhibited an approximate Gaussian spatial energy distribution. Computer procedures were used to control the position and length of the grooves. Different scan speeds and laser energies were used to study the formation of grooves. Scan speeds were varied from 50 to 500 mm s^{-1} with fixed laser energy of 0.5, 2, and 5 W, respectively, and the scanning number with these processing parameters was 10. Laser energy was varied from 0.5 to 5 W at a fixed scan speed of 50, 250, and 500 mm s^{-1}, and the scanning number with these processing parameters was 30. Machining processes were carried out in air atmosphere.

Noteworthy, energy fluence is an important processing parameter and is significantly related to the depth, width, and morphology of the grooves. The laser pulse energy (E_p) can be transformed into laser peak fluence (φ_0) of a Gaussian beam according to equation (1) as follows [20]:

$$\phi_0 = 2E_P/(\pi\omega^2) \quad (1)$$

where ω is the Gaussian laser beam-waist radius.

As a novel semiconductor material, the polymer derived SiAlCN ceramics exhibit incubation effect during laser processing [21]; therefore, the ablation threshold fluence bears a relationship with the effective number of pulses N_{eff} irradiated on the sample. At a certain scan speed ν with a pulse repetition rate of f, the N_{eff} could be expressed by using the following equation (2) [20]:

$$N_{\text{eff}} = \sqrt{\pi/2} \times f\omega/\nu \quad (2)$$

The spacing between pulses is much less than the spot radius ω. The N_{eff} is determined as the accumulated fluence per unit area of a Gaussian pulse profile which has a peak fluence φ_0.

3. Results and discussion

3.1. Effect of scan speed

During laser machining process of SiAlCN ceramics, different types of laser-induced ablation morphologies such as ablated zone, HAZ, and

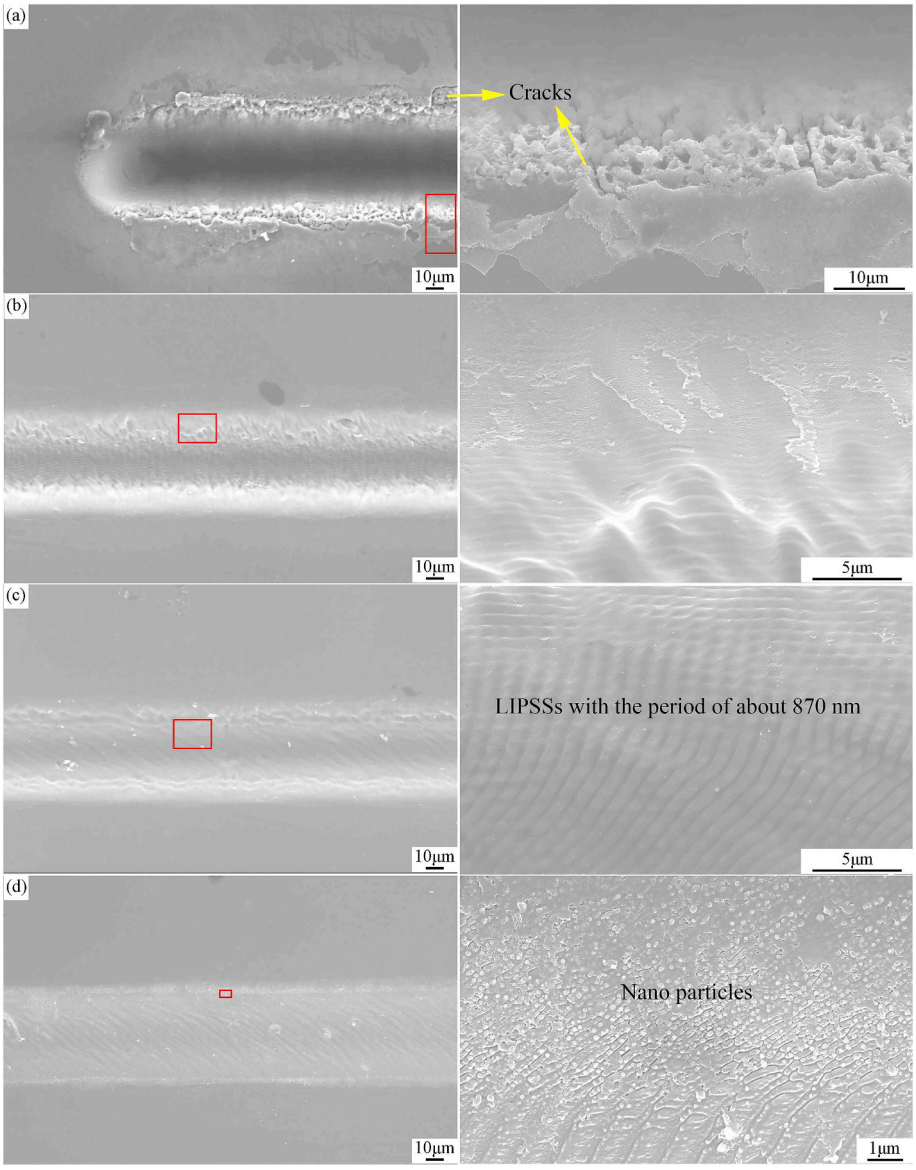

Fig. 2. SEM micrographs of the surface of laser-machined grooves at 4.57 J cm^{-2} and different scan speeds: (a) 50, (b) 150, (c) 250, and (d) 500 mm s^{-1}. Photos in right column are the enlarge photos of the labelled areas in left column.

surface microstructures are obtained with different laser parameters. Therefore, the laser parameters including scan speed and energy fluence are investigated for the comprehensive understanding of their influences on ablation of SiAlCN ceramics. The scan speed ranges from 50 to 500 mm s^{-1}, with a step size of 50 mm s^{-1}, corresponding to the N_{eff} range from ca. 42 to 4.2 for one-scan, respectively. The energy fluence is calculated according to equation (1), which is found to be in the range from 1.14 to 11.43 J cm^{-2}.

Fig. 1 shows the SEM micrographs of laser-machined groove with representative scan speed at energy fluence of 11.43 J cm^{-2}. Owing to high energy fluence, serious ablation occurs with low machining quality. With the increase of scan speed, the ablation degree and material removal are reduced. Further, when the scan speed is 50 mm s^{-1}, severe ablation with large material removal occurs in the laser-irradiated area. At the edge of grooves, a large amount of debris gets deposited and some cracks are also observed. And these areas are defined as HAZ as labelled in Fig. 1(a). However, at the scan speed of 150 mm s^{-1}, additional laser-induced stripes are formed at the bottom of grooves and the size of deposited particles decreased at the edge of grooves. As speed increased to 250 mm s^{-1}, the strips become unclear. Finally, high scan speed of 500 mm s^{-1} results in the formation of ablative traces with laser circular spot at the laser-irradiated surface as shown in Fig. 1(d). It is seen at energy fluence of 11.43 J cm^{-2}, intensive ablation process occurs, leading to the inevitable existence of HAZ, although it diminishes with the increase of scan speed as shown in Fig. 1(a)-1(d).

Fig. 2 shows SEM images of surface morphologies of laser-machined grooves with different scan speed at energy fluence of 4.57 J cm^{-2}. Compared to the laser-machined grooves obtained at energy fluence of 11.43 J cm^{-2}, the ablation degree at 4.57 J cm^{-2} is relatively weak. At 50 mm s^{-1}, the HAZ with some cracks and deposited debris is also observed at the edge of grooves. Fig. 2(a) presents coarse ablation microstructures at the edge of groove. Furthermore, Fig. 2(b)–(d) demonstrate that with the increase of scan speed, the machining damage is reduced, and then better quality of grooves without apparent cracks is obtained. At 250 mm s^{-1}, the LIPSSs with the period of about 870 nm are observed. With the increase of scan speed, the ablation degree decreases, resulting to the nanoparticles (NPs) formed at the periphery of LIPSSs as shown in Fig. 2(d). It is suggested that these randomly distributed nanostructures play an important role in the formation of

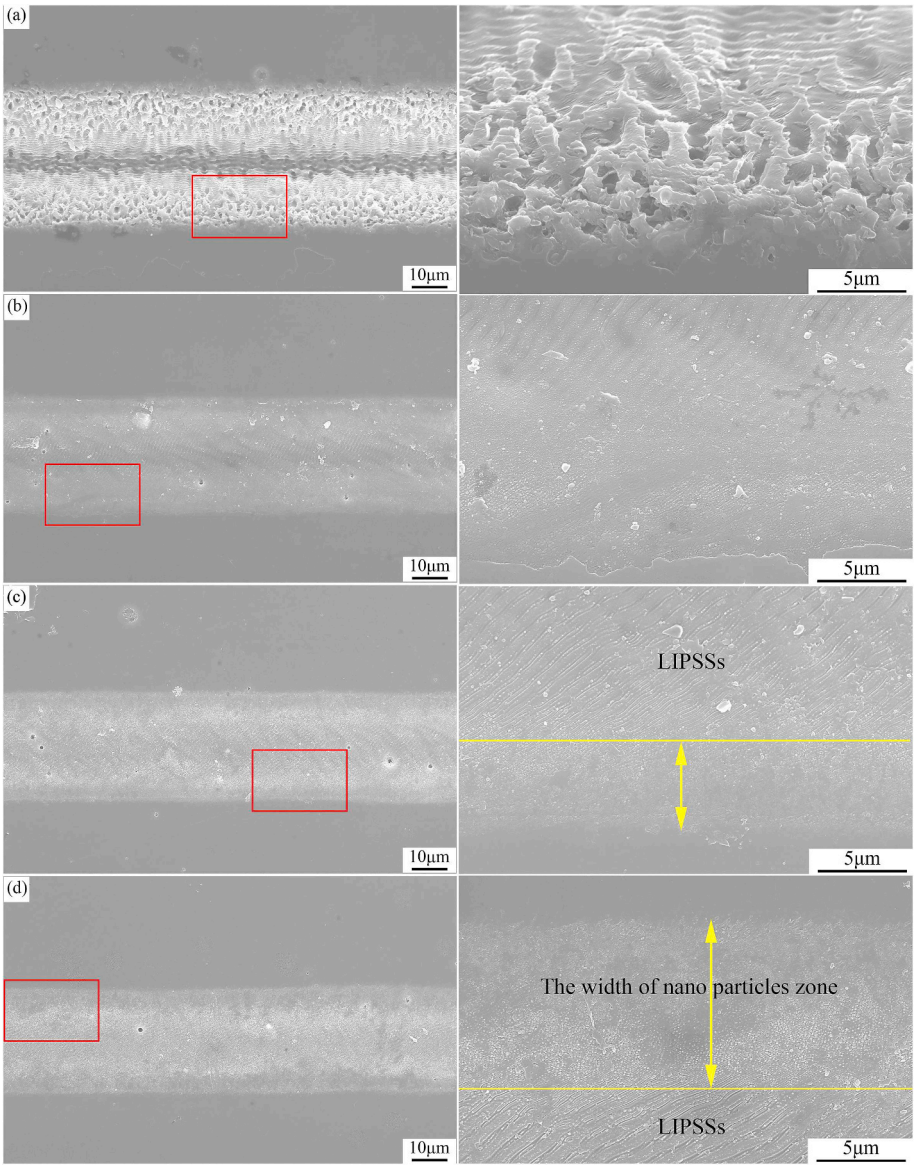

Fig. 3. SEM micrographs of the surface of laser-machined grooves at 1.14 J cm^{-2} and different scan speeds: (a) 50, (b) 150, (c) 250, and (d) 500 mm s^{-1}. Photos in right column are the enlarge photos of the labelled areas in left column.

LIPSSs due to their couple effect on the generation of surface plasmon polaritons (SPPs) [22].

Fig. 3 illustrates the surface morphologies of the laser-machined grooves with different scan speed at energy fluence of 1.14 J cm^{-2}. Fortunately, grooves without HAZ are obtained. At 50 mm s^{-1}, the ablation morphology is coarse at the edge, and some shallow LIPSSs are formed as indicated by Fig. 3(a). From Fig. 3(b)-3(d), it is seen the surface microstructures are mainly composed of the LIPSSs and NPs. Furthermore, Fig. 3(c) and (d) demonstrate that with the increase of scan speed, the ablation degree decreases and the width of NPs area gets wider in the laser-irradiated area. This indicates that the NPs are first generated at edge of laser-irradiated area with low laser energy. This phenomenon can be explained by the initial non-uniform laser energy deposition and localized nanoscale melts [23]. As a result, based on the investigation of scan speed at three energy fluences, the influence of scan speed on surface morphology and grooves quality are demonstrated. In certain energy fluences, high scan speed is suggested to fabricate high-quality grooves without HAZ.

Fig. 4 illustrates the cross-section morphology of laser-machined grooves at different scan speeds for three energy fluence of 1.14, 4.57, and 11.43 J cm^{-2}. Due to the Gaussian distribution of laser pulse, the cross-section profiles of grooves are clearly observed with Gaussian profiles. The depth and width of grooves are defined in the lower right corner of Fig. 4. Noteworthy, the width of grooves is almost constant at certain energy fluence. However, the depth of grooves exhibits huge distinction and is related to the scan speed and energy fluence. At low scan speed below 250 mm s^{-1} with 11.43 J cm^{-2}, the profiles of grooves are irregular and even the materials get ruptured or cracks are generated. More interestingly, a deep groove structure named 'branching' occurs at the bottom when the scan speed decreased to 100 mm s^{-1}. Similar result is also observed at the energy fluence of 4.57 J cm^{-2} and scan speed of 50 mm s^{-1}. This phenomenon can be explained by the Gaussian distribution nature of laser energy. Owing to the Gaussian distribution of laser energy, the greatest amount of laser energy will accumulation in the center, resulting in severer ablation. Then, branching rapidly occurs in the center with rapid removal of materials. In this study, severe ablation stage is defined as the stage when branching emerges. However, branching is not generated at low energy fluence of 1.14 J cm^{-2}, which may due to the insufficient energy accumulation. Moreover, the cross-section morphology of ablated depth is unclear when the scan speed is higher than 250 mm s^{-1} for this energy fluence. It could be treated as a mild ablation for the SiAlCN ceramics in this study. Besides, for stage where the grooves with apparent ablation morphology but without branching is defined as moderate ablation. Therefore, according to the cross-section morphologies of grooves, three different ablation stages are defined, namely mild ablation, moderate ablation, and severe ablation. Moderate ablation stage exhibits obvious Gaussian profiles of grooves, with laser parameters such as scan speed in the range from 100 to 500 mm s^{-1} at 4.57 J cm^{-2}, which is suitable for the groove fabrication.

The depth of all machined grooves is measured using a step profiler and confirmed by the cross-section SEM micrographs. Therefore, the range of depth for three ablation stage can be obtained in this study, namely mild ablation stage (below 5 μm), moderate ablation stage (5 μm < d < 75 μm) and severe ablation stage (75 μm < d < 280 μm), respectively. Fig. 5 exhibits the relationship between grooves depth and N_{eff} at three certain energy fluences. At 1.14 J cm^{-2}, the depth is relatively low and increases with N_{eff} as shown in Fig. 5(a). Mild ablation is dominated in the laser-machined grooves at 1.14 J cm^{-2} and moderate ablation occurs when N_{eff} is larger than 140. Since the ablation rate can be obtained via depth/pulse, a linear relationship is used to fit the mild stage as shown in the inserted picture in Fig. 5(a). The ablation rate for mild ablation is 37 nm/pulse. At 4.57 J cm^{-2}, majority points are located in the moderate ablation stage, except for the maximum depth of 150 μm in severe ablation stage. Therefore, the ablation rate with 239 nm/pulse in moderate ablation stage could be obtained through the linear fitting obtained from the inserted pictures in Fig. 5(b). As for 11.43 J cm^{-2}, the moderate ablation and severe ablation stages occur. A saturation depth of ~280 μm is obtained when N_{eff} is larger than 210. It is attribute to the diminishing of laser ablation when laser machined deep structures and the generation of branching, the relationship between grooves depth and N_{eff} in severe ablation stage is nonlinear which is not easy to fit in this study. However, the ablation rate with 468 nm/pulse

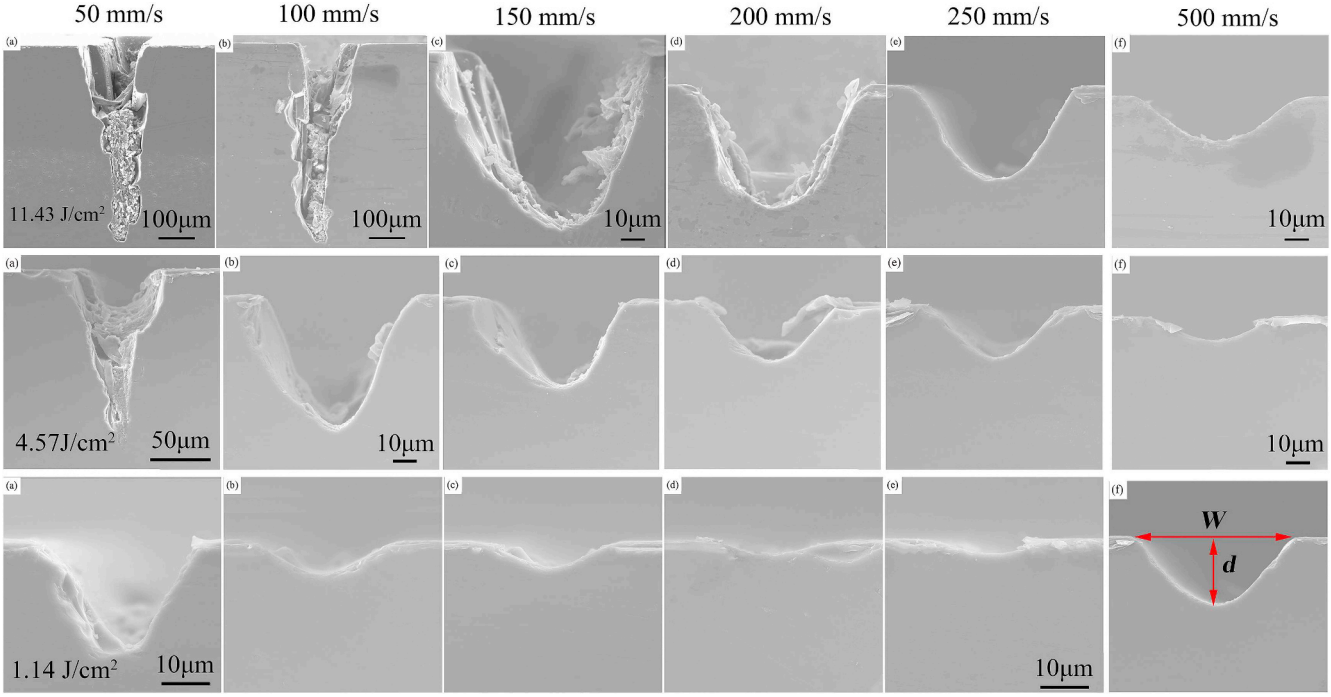

Fig. 4. Cross-section SEM microphotographs of the laser-machined grooves fabricated with different scan speed at three certain energy fluences (1.14, 4.57, and 11.43 J cm^{-2}). Inserted in the lower right corner: definition used herein for the width (W) and depth (d) of the grooves.

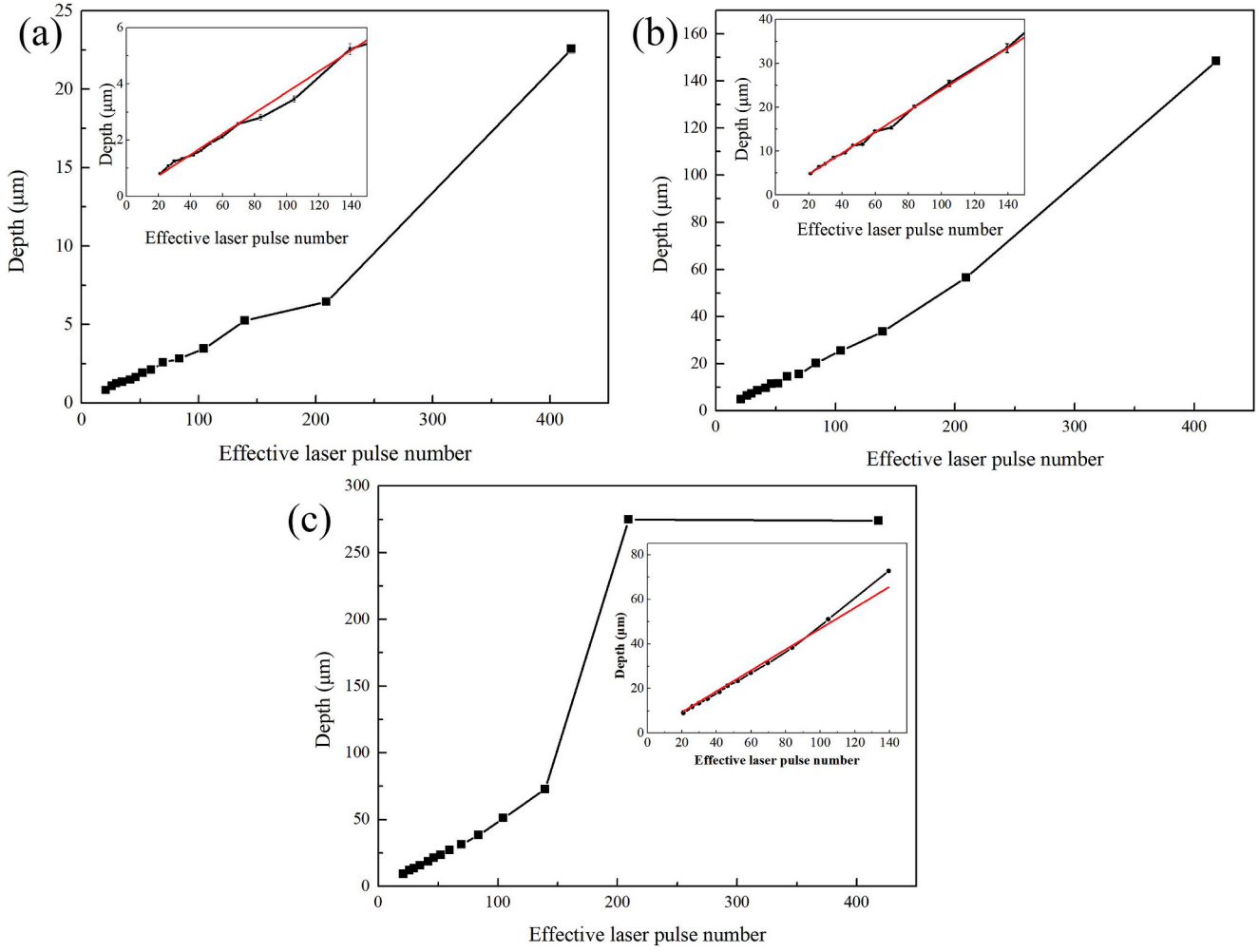

Fig. 5. Relationship between groove depth and the effective laser pulses number at different energy fluences: (a) 1.14, (b) 4.57, and (c) 11.43 J cm^{-2}

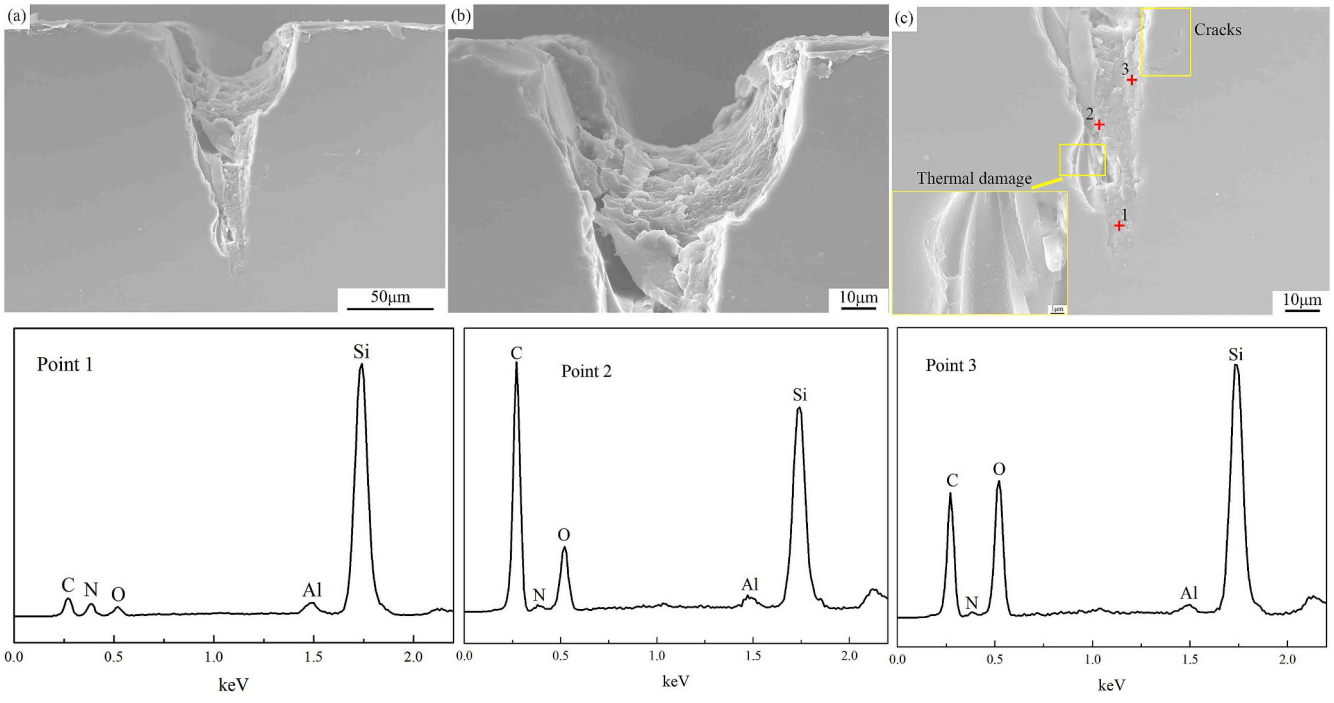

Fig. 6. SEM micrographs of grooves fabricated at 4.57 J cm^{-2}, 50 mm s^{-1} and the corresponding EDS patterns.

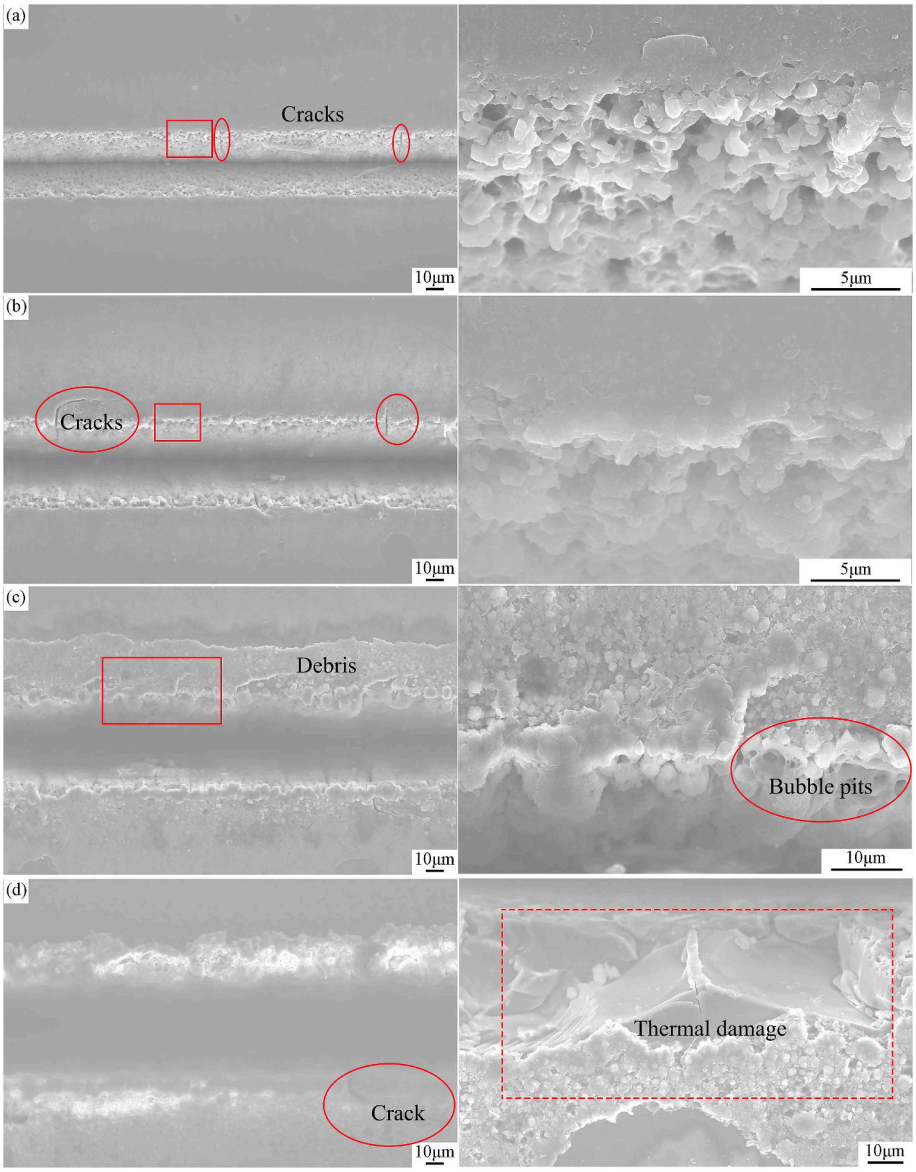

Fig. 7. SEM micrographs of laser-machined grooves with different energy fluences at 50 mm s^{-1}: (a) 1.14, (b) 2.28, (c) 4.57, and (d) 11.43 J cm^{-2}. Photos in right column are the enlarge photos of the labelled rectangle areas in left column.

in moderate stage can still be obtained from the inserted pictures Fig. 5(c). As mentioned above, moderate ablation stage is desirable for high-quality groove fabrication. Thus, for the moderate ablation stage, the ablation rate (depth/pulse) increases with the increasing energy fluence. Therefore, except for the influence of scan speed, energy fluence also plays an important role on the ablation characteristics of PDCs.

According to the ablation morphology above, the branching formed at the bottom of grooves attracts our attentions [24]. Fig. 6 shows the microstructures of branching under the condition of 4.57 J cm^{-2} and 50 mm s^{-1}. Fig. 6(b) shows incomplete Gaussian profiles at the upper half part. Furthermore, Fig. 6(c) exhibits that large amounts of debris are stacked at the groove bottom, in particular, in the bottom half part. In these deep structures, laser-induced plasma is formed at such high energy intensity, and it is difficult to eject out the plasma from these deep structures thus it remains at the bottom of grooves. Moreover, the laser energy is repeatedly absorbed by the remaining plasma and debris, thus diminishing further ablation [20]. Notably, the absorbed energy of plasma is converted into heat and transferred to inner layer, which results in cracks and thermal damage as shown in Fig. 6(c). Fig. 6 also exhibits the EDS patterns, indicating that the composition of point 1 at the lowermost part of branching shows an apparent decrease of C intensity, compared to the EDS of SiAlCN substrate illustrated in Fig. 3. Plasma movement is restricted in deep structures; thus, the laser-excited C atoms can be deposited, causing the increase of C peak intensity in point 2. However, with the increase in O concentration from inside to outside, the oxidation reaction occurs more easily. More C atoms react with oxygen to form gaseous products, showing a decrease of C peak intensity in point 3. Existence of other elements is attributed to the deposition of the restricted plasma and debris. Therefore, for fabricating a deep groove, high energy fluence and low scan speed are required. Moreover, the efficiency and timely removal of debris are also necessary in order to avoid machining defects.

3.2. Effects of energy fluence

A series of grooves is fabricated on the surface of SiAlCN ceramics with different energy fluences at three certain scan speeds (50, 250, and 500 mm s^{-1}). Fig. 7 shows the SEM micrographs of the top sides of groove machined at 50 mm s^{-1}. Different ablation phenomena are

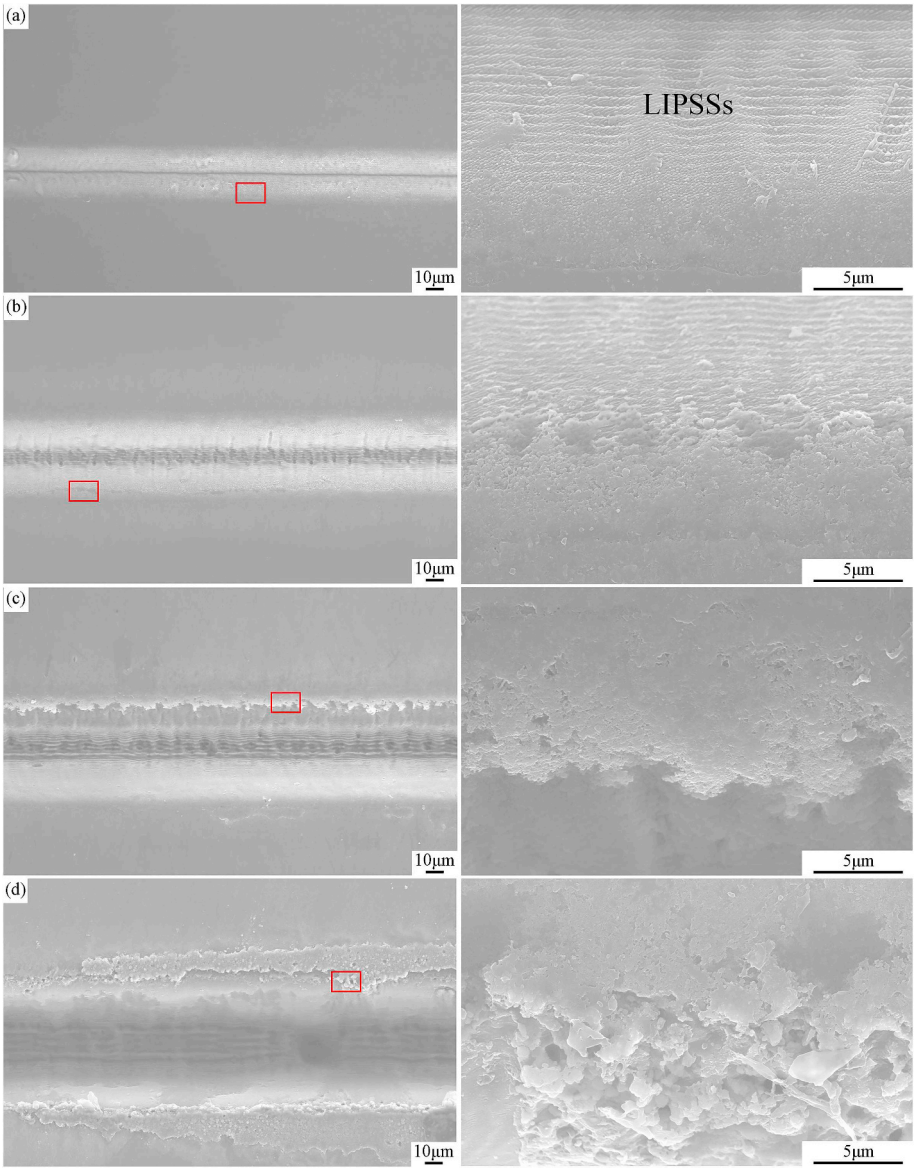

Fig. 8. SEM micrographs of the laser-machined grooves at different energy fluences at 250 mm s^{-1}: (a) 1.14, (b) 2.28, (c) 4.57, and (d) 11.43 J cm^{-2}. Photos in right column are the enlarge photos of the labelled rectangle areas in left column.

presented at four representative energy fluences of 1.14, 2.28, 4.57, and 11.43 J cm^{-2}, respectively. From the results of the SEM micrographs, the width and depth of grooves are enhanced with the increase of energy fluence. Fig. 7(a) exhibits the generation of some cracks, and adherence of many micro particles at the edge of groove. With the increase of energy fluence, the ablation becomes more serious. Fig. 7(b) exhibits the generation of more cracks, which then extend outward. At the edge of groove, the size of particles become larger which adheres at the side walls. At 4.57 J cm^{-2}, more debris are deposited at the edge of groove due to more material removal. Additional, some bubble pits are also formed due to the accumulation of laser energy. When energy fluence increases to 11.43 J cm^{-2} as shown in Fig. 7 (d), the material rupture induced by thermal damage and numerous deposited debris are observed at the edge of groove. It is clearly seen the unexpected HAZ is generated even at low energy fluence and become severer with the increase of energy fluence due to the excessive laser energy absorbed by SiAlCN ceramics, which results in the decrease of the machining quality of grooves.

Fig. 8 shows the morphological evolution of laser-machined grooves with four representative energy fluences at 250 mm s^{-1}. Similarly, the width of grooves gets wider with the increase of energy fluence. At low energy fluences, fortunately, the HAZ is not observed at the edge of grooves as shown in Fig. 8(a) and (b). The LIPSSs are formed at laser-irradiated area. However, with the enhancement of energy fluence, the LIPSSs become disordered until they disappear and the HAZ is formed as shown in Fig. 8(c) and (d). The debris deposited at the edge of grooves gradually increases and the morphology at the margin becomes coarser.

The laser-machined grooves with four representative energy fluences at scan speed of 500 mm s^{-1} are illustrated in Fig. 9. Clearly, the width of grooves increases and fortunately HAZ is not found in all laser-machined grooves. However, surface microstructures present huge distinction at different energy fluences. Some NPs are distributed at the rim of groove as shown in Fig. 9(a) and (b), corresponding to the results in Fig. 3. The number of NPs at the edge of groove is decreased and more LIPSSs are formed when the energy fluence is 4.57 J cm^{-2}. At all laser-machined grooves with high scan speed, LIPSSs are dominant in the surface morphology and their direction often changes and finally becomes parallel to the scan direction of laser beam as shown in Fig. 9(d), which will be discussed in the next section.

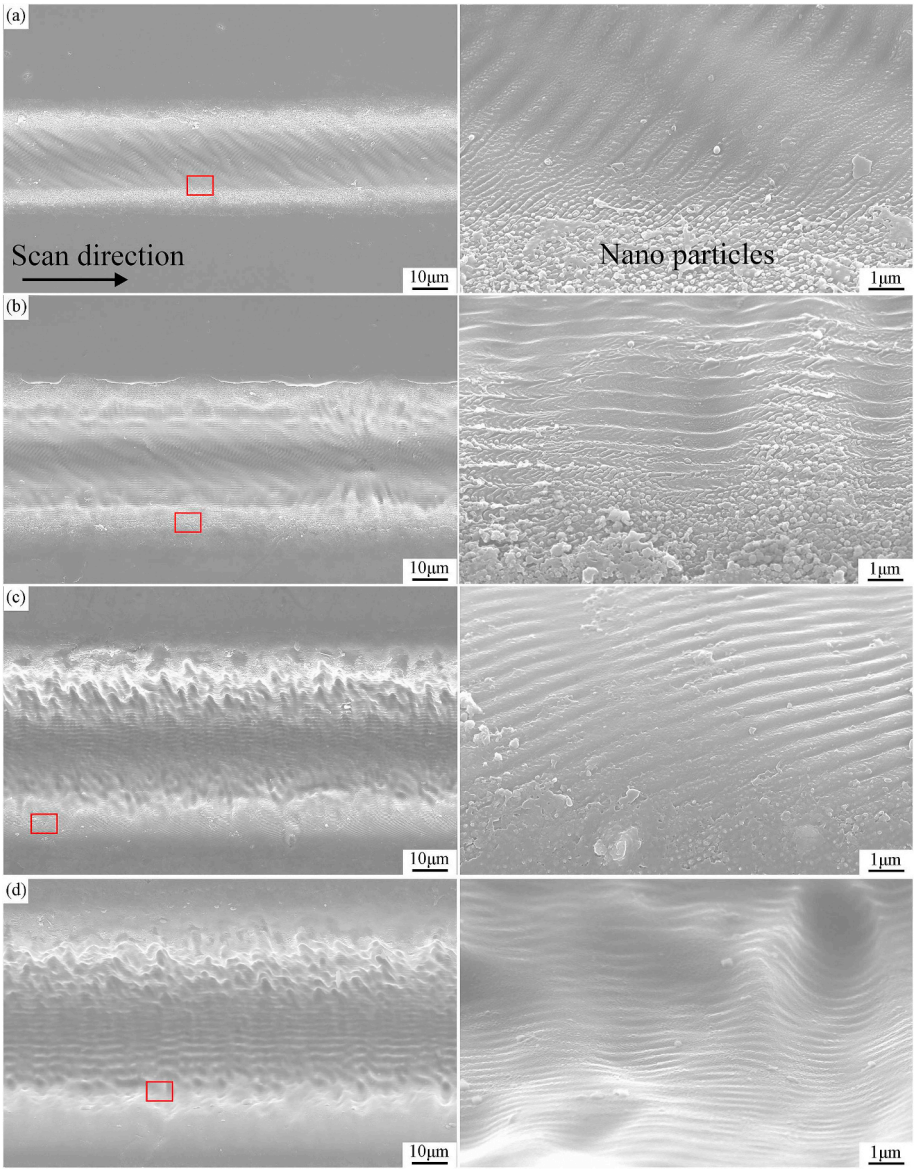

Fig. 9. SEM micrographs of the laser-machined grooves with different energy fluences at 500 mm s^{-1}: (a) 1.14, (b) 2.28, (c) 4.57, and (d) 11.43 J cm^{-2}. Photos in right column are the enlarge photos of the labelled rectangle areas in left column.

Fig. 10 presents the evolution of cross-section morphologies of laser-machined grooves with different energy fluences at three certain scan speeds (50, 250, and 500 mm s^{-1}). At 50 mm s^{-1}, severe ablation occurs and a branching is formed at the groove bottom except at 1.14 J cm^{-2}. The depth of grooves increases with the increasing of energy fluence. Moreover, the ablated morphology of the cross-section is rather coarse and material rupture induced by excessive heat accumulation can be observed clearly. However, the branching is not formed at 250 mm s^{-1}. Significant removal of materials resultes in deposition of large amounts of debris on the bottom of grooves, which is clearly illustrated in the cross-section SEM micrographs. Nonetheless, at 500 mm s^{-1}, all laser-machined grooves exhibits a Gaussian profile with no significant HAZ and debris at the bottom of grooves. Therefore, the variation of energy fluences could induce rapid changes in the grooves' morphology and the width and depth of grooves.

The width and depth of the laser-machined grooves with different energy fluences at scan speed of 50, 250, and 500 mm s^{-1} are also measured and presented as a function of energy fluence as shown in Fig. 11. At different scan speeds, the width of grooves varies significantly from ~30 to ~75 μm, corresponding to the change of energy fluence from 1.14 to 11.43 J cm^{-2}. This variation could be explained by the Gaussian distribution of laser beam energy. When the energy fluence is increased, the energy at the periphery of laser beam is also increased, as well as the increased ablation, and strong distortion and divergence of the laser beam [25], inducing the growth of grooves width. The groove width tends to saturate with the increase of energy fluence due to the limitation of laser spot size, reaching approximately 75 μm. Similar to the variation of groove width, the depth of grooves also increases with the increase of energy fluence. At 50 mm s^{-1}, the maximum ablation depth with ~250 μm reaches saturation at high energy fluence due to the limitation in the fabrication of deep-groove microstructures at this laser parameter. The groove depth reaches ~125 μm at 250 mm s^{-1}. Fortunately, at the scan speed of 500 mm s^{-1}, the branching does not occur and its maximum depth is about 55 μm, which is suitable for the fabrication of grooves with high quality. In addition, all of the laser-machined grooves depth is higher than 5 μm with the occurrence of moderate ablation and severe ablation, which is attributed to the increase of scan number from 10 to 30. More laser energies are absorbed by SiAlCN ceramics and the depth of grooves enhances. However, once the branching generates, the laser ablation

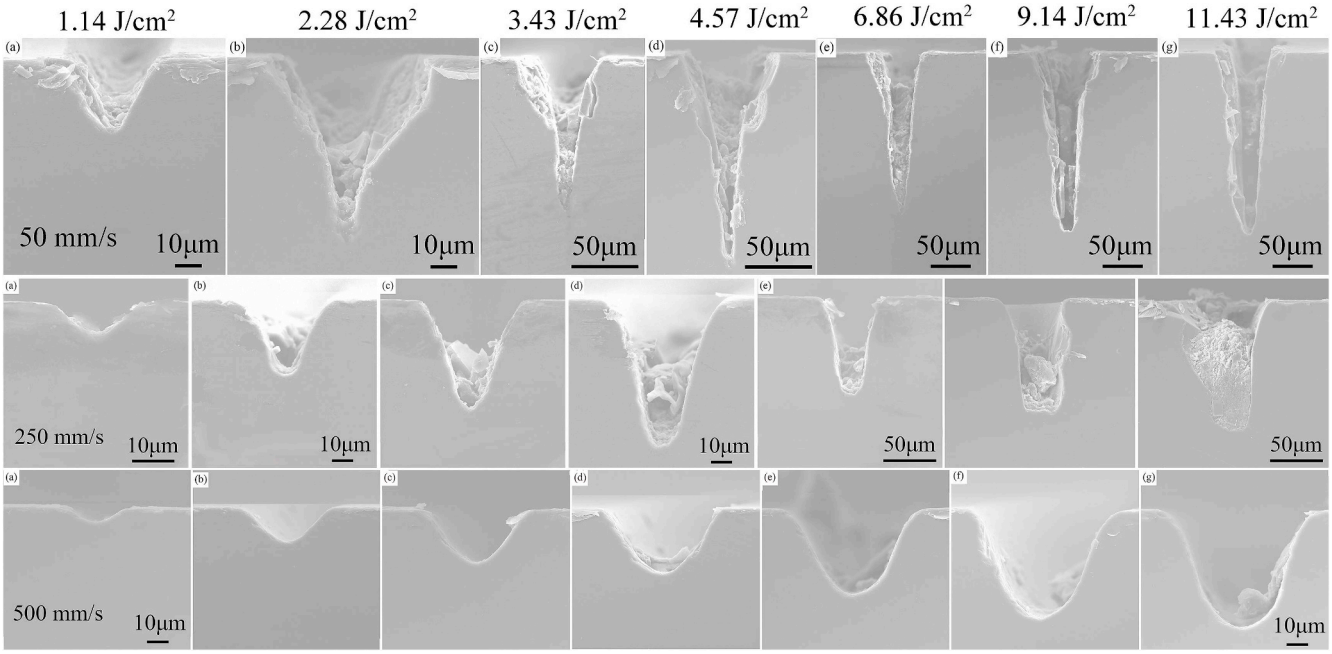

Fig. 10. SEM micrographs of laser-machined grooves produced using different energy fluences: (a) 1.14, (b) 2.28, (c) 3.43, (d) 4.57, (e) 6.86, (f) 9.14, and (g) 11.43 J cm^{-2}.

exhibits nonlinear relationship when laser machined deep structures. Therefore, for more attention is focused on the occurrence of moderate ablation stage.

According to the investigation of the scan speed and energy fluence on the laser-machined grooves, the formation of HAZ plays an important role in deciding the machining quality of SiAlCN ceramics, which induces the deposition of debris as well as the generation of cracks or material rupture. The HAZ is generated around the grooves due to high laser energy fluence, intense laser-material interaction, and rapid condensation [26]. Therefore, in order to obtain laser-machined grooves with high quality, avoidance of the generation of HAZ is required. Fig. 12 exhibits the SEM micrographs of HAZ at the edge of grooves. Fig. 12(b) demonstrates that in the HAZ, large amounts of micro-spheres and cracks induced by thermal damage are present. Fig. 12(c) shows that at the inner side of grooves, a porous layer with many bubble pits is present. This porous layer works as exit channels of gaseous products during laser machining. The amorphous structure of SiAlCN ceramics and the EDS patterns shown in Fig. 12 together indicate that the gaseous products may be the oxides of nitrogen and carbon. Moreover, this layer is only found at the most intense ablated grooves such as at the condition of 50 mm s^{-1} and 11.43 J cm^{-2}. From the edge of grooves to the far away region, four points EDS patterns are examined as presented in Fig. 12(b). The results show that the debris deposited in HAZ is composed of Si, O, C, and Al. The N atoms are released during the laser-machining and the Al atoms are oxidized to Al_2O_3. Some un-reacted C is also deposited after laser ablation in the absence of oxygen. The result of EDS pattern shows a spot of C and more content of O at the point 3, due to sufficient reaction at farther area between the laser-induced plasma and air environment. Only some debris sputters to the point 4 containing N element and relatively high content of O element. Thus, it could be treated as an unaffected region. Therefore, three parts of surface region are obtained, including ablated region, HAZ, and unaffected region. In Fig. 12(d) the width of HAZ is defined. Noteworthy, it is important to optimize the laser parameters in order to avoid the formation of HAZ. Fig. 13 shows the width of HAZ around the laser-machined groove at different laser parameters. At 11.43 J cm^{-2} or 50 mm s^{-1}, the HAZ is inevitably generated; however, its width decreases with the increase of scan speed or decrease of energy fluences, respectively. When the energy fluence is 4.57 J cm^{-2} or scan speed is 250 mm s^{-1}, notably, a formation threshold of HAZ is obtained. Then, it rapidly increases with the decrease of scan speed or the increase of energy fluences. Fortunately, the HAZ is not formed in all laser-machined grooves at 500 mm s^{-1} or at 1.14 J cm^{-2}. Therefore, the laser parameters with high scan speed or low energy fluences are useful to avoid the formation of HAZ on SiAlCN ceramics.

3.3. Formation and disappearance of laser-induced periodic surface structures

During laser processing in SiAlCN ceramics, the LIPSSs or ripples, as common and significant microstructures, are formed on the laser-irradiated area. Till date, several theories are used to interpret their formation; nonetheless, the resonant mechanisms seem to be the most dominant [27]. It is related to the plasmon excitation on surface and periodic energy deposition based on electromagnetic aspects. In general, during the first few laser pulses, some surface nanostructures are randomly produced. Then, these nanostructures couple with the next laser light to generate SPPs [21]. The polarized laser beam then interferes with SPPs, causing a periodic spatial modulation of energy deposited in the laser-irradiated area [28]. Spatially modulated heating is responsible for the generation of surface periodic structures on the laser-irradiated area. Based on all the morphological characteristics of surface of laser-machined grooves, the formation process of LIPSSs is demonstrated in Fig. 14. At low energy fluence or high scan speed, numerous NPs are first formed based on the melting effect of laser pulse, which is often observed at the edge of grooves. Then, Fig. 14(b) demonstrates that under the interference between the polarized laser beam and SPPs, these NPs are gradually uniformly distributed. This may be the evidence of rudimentary LIPSSs that result from the deposition and aggregation of NPs [29]. Fig. 14(d) shows the changing process from NPs to LIPSSs. NPs get linked with each other and generate the LIPSSs. It is thus indicated that NPs play an important role in the formation of LIPSSs.

With the increase of energy fluence, the ablation becomes a dominant process and the LIPSSs gradually disappear from the irradiated area as shown in Fig. 15. Fig. 15(a) demonstrates that LIPSS with period of about 870 nm is generated and its direction is inclined to the scan direction. Clearly, some NPs are still adhered on the surface of LIPSSs.

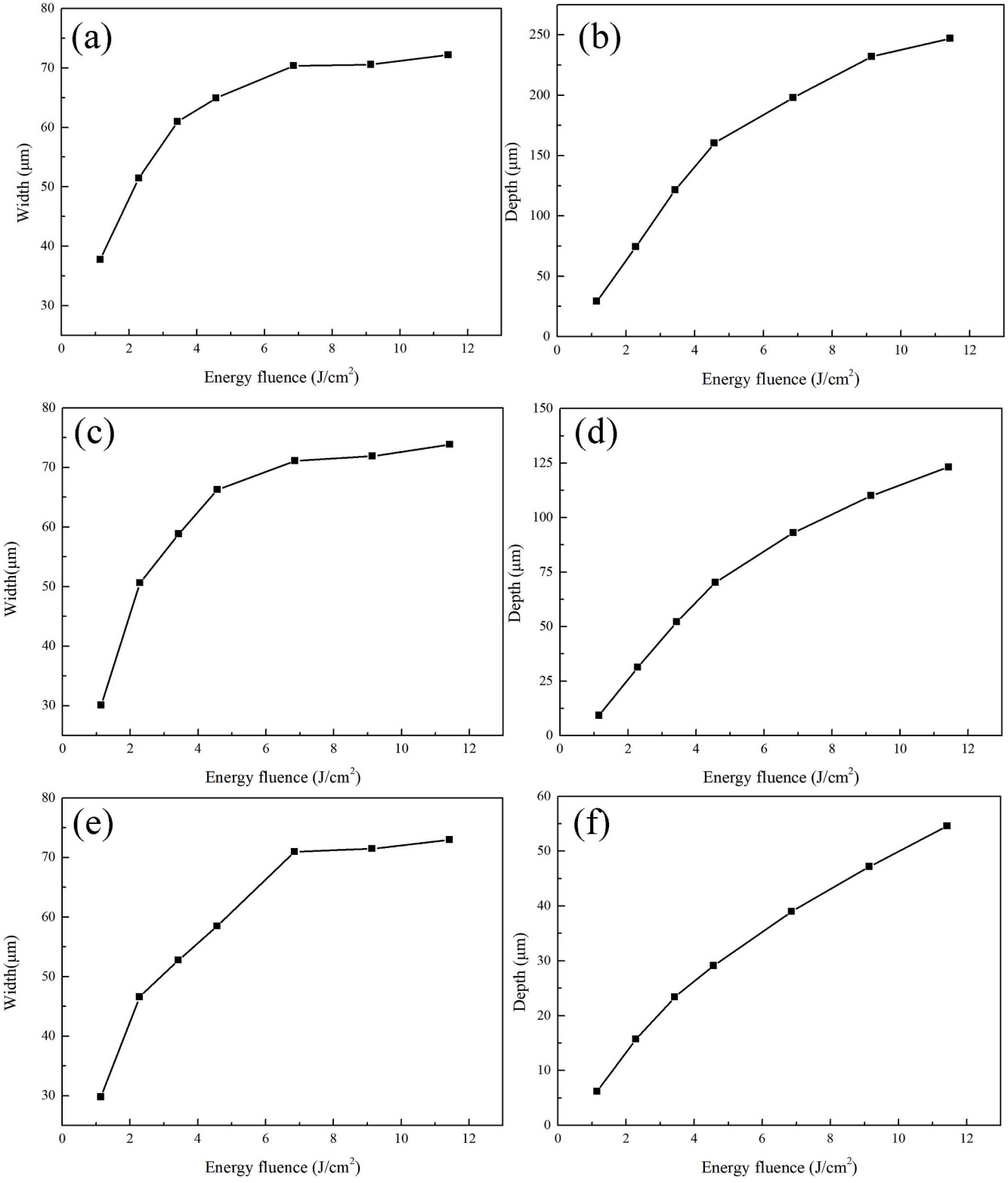

Fig. 11. The depth and width of grooves as a function of energy fluence: (a and b) 50 mm s^{-1}, (c and d) 250 mm s^{-1}, and (e and f) 500 mm s^{-1}.

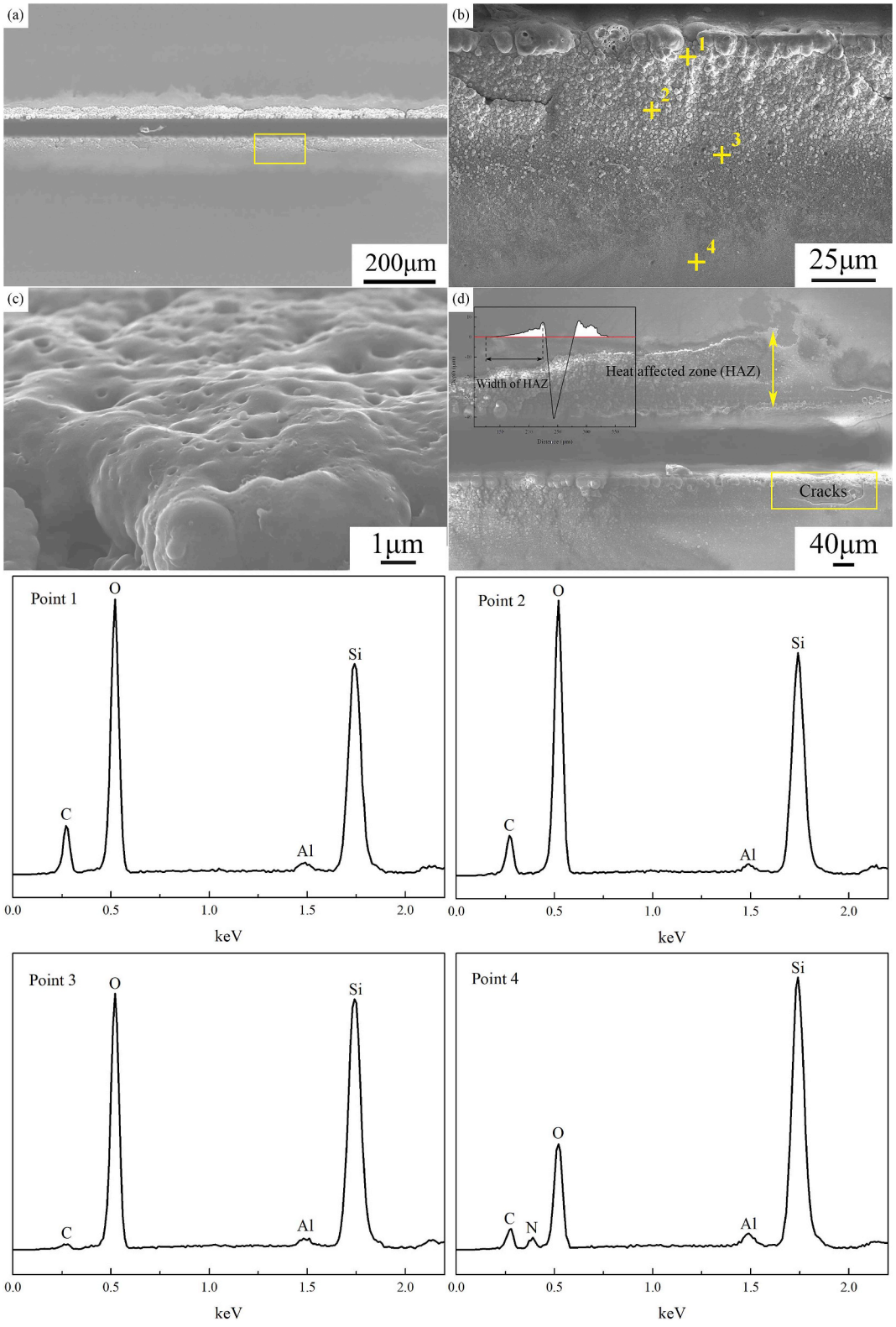

Fig. 12. SEM microphotographs of groove: (a) groove fabricated with energy fluence of 11.43 J cm^{-2}, scan speed of 50 mm s^{-1}, (b) enlarged SEM micrograph corresponding to (a) and EDS at the edge of HAZ (four points), (c) a porous layer at inner side of grooves, and (d) definition of HAZ around the grooves.

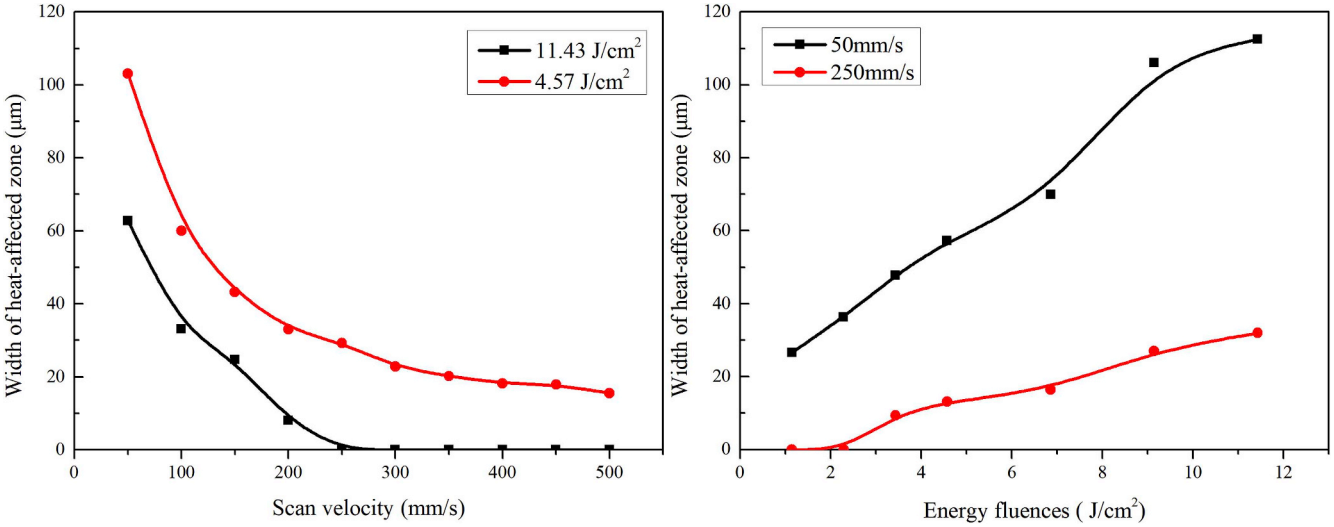

Fig. 13. Width of HAZ around the laser-machined groove under different laser parameters.

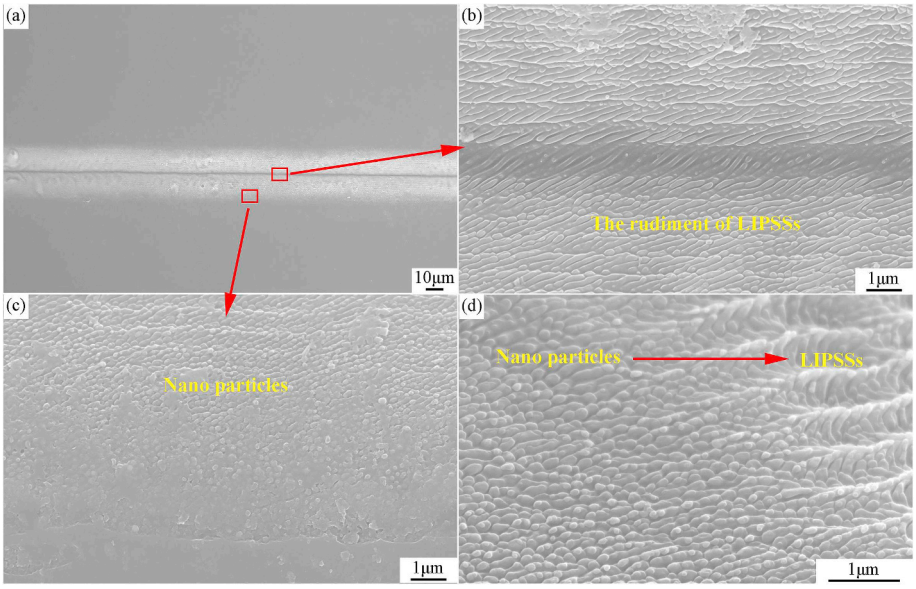

Fig. 14. SEM micrographs of the formation of LIPSSs under the condition of 250 mm s^{-1} and 1.14 J cm^{-2}.

When the energy fluence is 3.43 J cm^{-2}, the surface morphology becomes coarse and then two types of LIPSSs coexist at the bottom of grooves as shown in Fig. 15(b). Then, the LIPSSs with a direction paralleled to scan direction mainly become dominant as illustrated in Fig. 15(c). For all laser-machined grooves, with the increase of ablation degree, the direction of LIPSSs at the bottom of grooves is finally parallel to the scan direction. The formation of parallel LIPSSs is the result of the restriction of laser-induced plasma due to the existence of groove walls [30]. Additionally, the mean spacing of parallel LIPSSs grows gradually with the energy fluence. Moreover, the LIPSSs become disorder until they disappear as shown in Fig. 15(d). The disappearance of LIPSSs is attributed to intense ablation with the enhancement of material removal. Therefore, the formation of LIPSSs on SiAlCN ceramics is ascribed to the interference between the laser beam and SPPs and its disappearance is caused by the enhancement of material removal.

4. Conclusion

In this study, grooves with a width in the range of 30–80 μm and a depth below 280 μm on SiAlCN ceramics surface were successfully fabricated using femto-second laser pulse with different laser energy and scan speed. The energy fluences and scan speed exhibited significant influence on the surface quality of grooves. The energy fluences below 4.57 J cm^{-2} and scan speed above 250 mm s^{-1} were found to be appropriate for fabricating good quality grooves. In severe ablation stage, the HAZ with cracks and deposited debris was generated. Branching was formed at the bottom of groove, which easily induced severe thermal damage in the inner layer. Moreover, formation of LIPSSs was attributed to the interference between the laser beam and SPPs and its disappearance occurred in more intense ablation stage because of more removal of ablated material. Three ablation stages with different microstructures were presented herein as shown in Fig. 16, which can be effectively used for further investigation of the SiAlCN ceramics machined via femtosecond laser pulse.

Declaration of competing interest

We state the work described here is an original research that has not

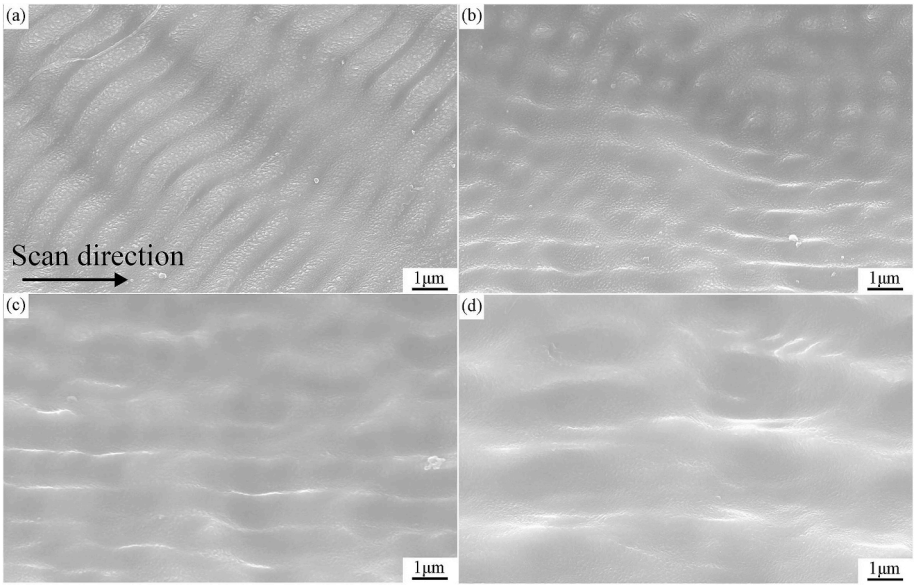

Fig. 15. SEM micrographs of the disappearance of LIPSSs at 500 mm s^{-1} and at different energy fluences: (a) 1.14, (b) 3.43, (c) 6.85, and (d) 11.43 J cm^{-2}.

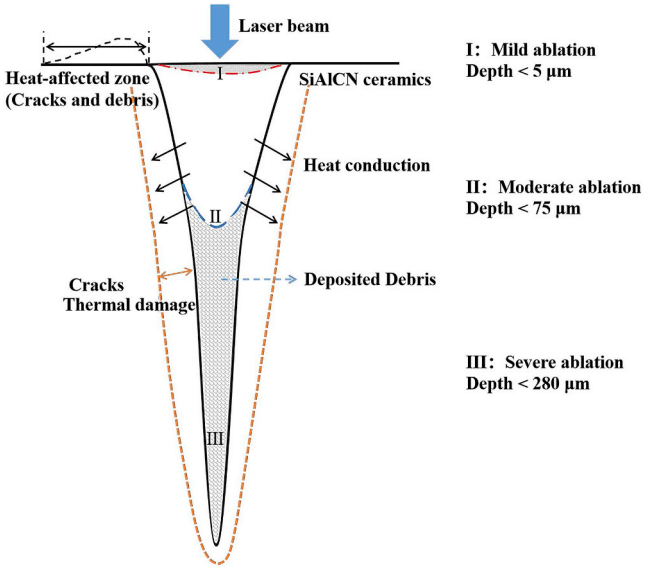

Fig. 16. Schematic illustration of femtosecond laser process of the SiAlCN ceramics.

been submitted elsewhere for publication, in whole or in part. No conflict of interest exits in the submission of this manuscript, and manuscript is approved by all authors for publication.

Acknowledgement

The authors acknowledge the support of the National Key Basic Research Program of China (Grant# 2015CB057400), the CAS equipment project (No. YJKYYQ 20180045), Natural Science Foundation of Shaanxi Province of China (grant number 2019JQ-540); the Fundamental Research Funds for the Central Universities.

References

[1] P. Colombo, G. Mera, R. Riedel, Gian Domenico Sorarù, Polymer-derived ceramics: 40 years of research and innovation in advanced ceramics, J. Am. Ceram. Soc. 93 (2010) 33.
[2] N. Li, Y.J. Cao, R. Zhao, Y. Xu, L.N. An, Polymer-derived SiAlOC ceramic pressure sensor with potential for high-temperature application, Sensor. Actuat. A-Phys. 263 (2017) 174–178.
[3] L.A. Liew, W. Zhang, V.M. Bright, L.N. An, M.L. Dunn, R. Raj, Fabrication of SiCN ceramic MEMS using injectable polymer-precursor technique, Sensor. Actuat. A-Phys. 89 (2001) 64–70.
[4] D.H. Lee, K.H. Park, L.Y. Hong, D.P. Kim, SiCN ceramic patterns fabricated by soft lithography techniques, Sensor. Actuat. A-Phys. 135 (2007) 895–901.
[5] N. Takayama, J. Yan, Mechanisms of micro-groove formation on single-crystal diamond by a nanosecond pulsed laser, J. Mater. Process. Technol. 243 (2017) 299–311.
[6] Y. Zou, G.Z. Yang, W.J. Zhang, J. Hu, Investigating the effect of picosecond laser texturing on microstructure and biofunctionalization of titanium alloy, J. Mater. Process. Technol. 255 (2018) 129–136.
[7] Y. Liu, L. Liu, J. Deng, R. Meng, X. Zou, F. Wu, Fabrication of micro-scale textured grooves on green ZrO_2 ceramics by pulsed laser ablation, Ceram. Int. 43 (2017) 6519–6531.
[8] X. Jia, T.Q. Jia, Y. Zhang, P.X. Xiong, Z.Z. Xu, Periodic nanoripples in the surface and subsurface layers in ZnO irradiated by femtosecond laser pulses, Opt. Lett. 35 (2010) 1248–1250.
[9] K.C. Vishnubhatla, N. Bellini, R. Ramponi, G. Cerullo, R. Osellame, Shape control of microchannels fabricated in fused silica by femtosecond laser irradiation and chemical etching, Optic Express 17 (2009) 8685–8695.
[10] S. Darvishi, T. Cubaud, J.P. Longtin, Ultrafast laser machining of tapered microchannels in glass and PDMS, Optic Laser. Eng. 50 (2012) 210–214.
[11] J.W. Kwon, E.S. Kim, Multi-level microfluidic channel routing with protected convex corners, Sensor. Actuat. A-Phys. 97 (2002) 729–733.
[12] P. Dittrich, R. Bartlome, G. Montemezzani, P. Günter, Femtosecond laser ablation of DAST, Appl. Surf. Sci. 220 (2003) 88–95.
[13] S. Nikumb, Q. Chen, C. Li, H. Reshef, H.Y. Zheng, H. Qiu, D. Low, Precision glass machining, drilling and profile cutting by short pulse lasers, Thin Solid Films 477 (2005) 216–221.
[14] B.C. Chen, Y.H. Tsai, C.Y. Ho, C.S. Chen, C. Ma, Parametric effects on femtosecond laser ablation of Al_2O_3 ceramics, Ceram. Int. 39 (2013) S341–S344.
[15] B. Sallé, O. Gobert, P. Meynadier, M. Perdrix, G. Petite, A. Semerok, Femtosecond and picosecond laser microablation: ablation efficiency and laser microplasma expansion, Appl. Phys. A-Mater. 69 (1999) S381–S383.
[16] B.N. Chichkov, C. Momma, S. Nolte, F. Von Alvensleben, A. Tünnermann, Femtosecond, picosecond and nanosecond laser ablation of solids, Appl. Phys. A-Mater. 63 (1996) 109–115.
[17] L. Romoli, G. Tantussi, G. Dini, Experimental approach to the laser machining of PMMA substrates for the fabrication of microfluidic devices, Optic Laser. Eng. 49 (2011) 419–427.
[18] T.H.R. Crawford, A. Borowiec, H.K. Haugen, Femtosecond laser micromachining of grooves in silicon with 800 nm pulses, Appl. Phys. A-Mater. 80 (2005) 1717–1724.
[19] Y.G. Wang, L.N. An, Y. Fan, L. Zhang, S. Burton, Z. Gan, Oxidation of polymer-derived SiAlCN ceramics, J. Am. Ceram. Soc. 88 (2005) 6.
[20] A. Borowiec, H.K. Haugen, Femtosecond laser micromachining of grooves in indium phosphide, Appl. Phys. A-Mater. 79 (2004) 521–529.
[21] J. Bonse, J.M. Wrobel, J. Krüger, W. Kautek, Ultrashort-pulse laser ablation of indium phosphide in air, Appl. Phys. A-Mater. 72 (2001) 89–94.
[22] A.V. Zayats, I.I. Smolyaninov, Near-field photonics: surface plasmon polaritons and localized surface plasmons, J. Opt. A-Pure. Appl. Op. 5 (2003) S16–S50.
[23] A.Y. Vorobyev, C.L. Guo, Femtosecond laser nanostructuring of metals, Optic Express 14 (2006) 2164–2169.
[24] A. Pan, J. Si, T. Chen, Y. Ma, F. Chen, X. Hou, Fabrication of high-aspect-ratio grooves in silicon using femtosecond laser irradiation and oxygen-dependent acid

etching, Optic Express 21 (2013) 16657.
[25] H.W. Kang, H. Lee, S. Chen, A.J. Welch, Enhancement of bovine bone ablation assisted by a transparent liquid layer on a target surface, IEEE J. Quant. Electron. 42 (2006) 633–642.
[26] Y.Q. Xing, J.X. Deng, X.T. Feng, S. Yu, Effect of laser surface texturing on Si_3N_4/TiC ceramic sliding against steel under dry friction, Mater. Des. 52 (2013) 234–245.
[27] J.E. Sipe, J.F. Young, J.S. Preston, H.M.V. Driel, Laser-induced periodic surface structure. i. theory, Phys. Rev. B Condens. Matter 27 (1983) 1141–1154.
[28] A.Y. Vorobyev, V.S. Makin, C. Guo, Periodic ordering of random surface nanostructures induced by femtosecond laser pulses on metals, J. Appl. Phys. 101 (2007) 034903.
[29] S. He, J.J. Nivas, K.K. Anoop, A. Vecchione, M. Hu, R. Bruzzese, S. Amoruso, Surface structures induced by ultrashort laser pulses: formation mechanisms of ripples and grooves, Appl. Surf. Sci. 353 (2015) 1214–1222.
[30] S.H. Kim, I.B. Sohn, S. Jeong, Parallel ripple formation during femtosecond laser grooving of ceramic, Appl. Phys. A-Mater. 103 (2010) 1053–1057.